Journal of Visualized Experiments

Evaluating Regional Pulmonary Deposition Using Patient-Specific 3D Printed Lung Models

--Manuscript Draft--

Article Type:	Invited Methods Article - JoVE Produced Video
Manuscript Number:	JoVE61706R1
Full Title:	Evaluating Regional Pulmonary Deposition Using Patient-Specific 3D Printed Lung Models
Section/Category:	JoVE Bioengineering
Keywords:	drug delivery; personalized medicine; 3D printing; pulmonary deposition; anatomical models
Corresponding Author:	Catherine Fromen University of Delaware Newark, DE UNITED STATES
Corresponding Author's Institution:	University of Delaware
Corresponding Author E-Mail:	cfromen@udel.edu
Order of Authors:	Emma Peterman
	Emily Kolewe
	Catherine Fromen
Additional Information:	
Question	**Response**
Please indicate whether this article will be Standard Access or Open Access.	Standard Access (US$2,400)
Please indicate the **city, state/province, and country** where this article will be **filmed**. Please do not use abbreviations.	Newark, DE, USA

Cover Letter

UNIVERSITY OF DELAWARE | Department of Chemical & Biomolecular Engineering

Catherine Fromen, Assistant Professor
150 Academy St. Newark, DE 19702
phone: (302) 831-3649
email: cfromen@udel.edu

July 20, 2020

Vineeta Bajaj, Ph.D.
Review Editor
JOVE
1 Alewife Center Suite 200
Cambridge MA 02140
benjamin.werth@jove.com

Re: Manuscript Revisions to "Evaluating Regional Pulmonary Deposition Using Patient-Specific 3D Printed Lung Models"

Dear Dr. Bajaj,

Please find the revised manuscript entitled "Evaluating Regional Pulmonary Deposition Using Patient-Specific 3D Printed Lung Models" by E. Peterman, E. Kolewe, and C. Fromen for your consideration in *JOVE*. This manuscript builds on ongoing work in our laboratory to develop upper airway models to study aerosol deposition in the lung. This protocol represents original research which has not been submitted elsewhere for publication. A complementary publication leveraging this experimental protocol has recently been accepted at the *Journal of Aerosol Medicine and Pulmonary Drug Delivery*.

We have responded to the reviewer comments in the attached response document and are submitting our revised manuscript. Both a tracked changes version and final clean copy have been uploaded.

We thank you for your time and consideration of this manuscript and look forward to your response.

Sincerely,

Catherine Fromen, PhD
Assistant Professor, University of Delaware

TITLE:

Evaluating Regional Pulmonary Deposition Using Patient-Specific 3D Printed Lung Models

AUTHORS AND AFFILIATIONS:

Emma L. Peterman[1], Emily L. Kolewe[1], Catherine A. Fromen[1]

[1]Department of Chemical and Biomolecular Engineering, University of Delaware, Newark DE, USA

Corresponding author:
Catherine A. Fromen (cfromen@udel.edu)

Email addresses of authors:
Emma L. Peterman (emmap@udel.edu)
Emily L. Kolewe (ekolewe@udel.edu)

KEYWORDS:

drug delivery, personalized medicine, 3D printing, pulmonary deposition, anatomical models, in vitro model, lobe-specific

SUMMARY:

We present a high-throughput, in vitro method for quantifying regional pulmonary deposition at the lobe level using CT scan-derived, 3D printed lung models with tunable air flow profiles.

ABSTRACT:

Development of targeted therapies for pulmonary diseases is limited by the availability of preclinical testing methods with the ability to predict regional aerosol delivery. Leveraging 3D printing to generate patient-specific lung models, we outline the design of a high-throughput, in vitro experimental setup for quantifying lobular pulmonary deposition. This system is made with a combination of commercially available and 3D printed components and allows the flow rate through each lobe of the lung to be independently controlled. Delivery of fluorescent aerosols to each lobe is measured using fluorescence microscopy. This protocol has the potential to promote the growth of personalized medicine for respiratory diseases through its ability to model a wide range of patient demographics and disease states. Both the geometry of the 3D printed lung model and the air flow profile setting can be easily modulated to reflect clinical data for patients with varying age, race, and gender. Clinically relevant drug delivery devices, such as the endotracheal tube shown here, can be incorporated into the testing setup to more accurately predict a device's capacity to target therapeutic delivery to a diseased region of the lung. The versatility of this experimental setup allows it to be customized to reflect a multitude of inhalation conditions, enhancing the rigor of preclinical therapeutic testing.

INTRODUCTION:

Many pulmonary diseases such as lung cancer and chronic obstructive pulmonary disease (COPD) exhibit regional differences in disease characteristics; however, there are a lack of therapeutic techniques available to target drug delivery to only diseased regions of the lung[1]. Multiple

computational fluid dynamic (CFD) models have demonstrated that it is possible to modulate drug deposition profiles by identifying specific streamlines in the lung[2,3]. Development of both inhalers and endotracheal (ET) tube adaptors with regional targeting capabilities are on-going in our lab to control aerosol distribution to diseased lung regions. Extension of these principles to clinical use is limited by current preclinical testing capacity. The precise location a drug deposits within the lung is known to be the best predictor of efficacy; however, current pharmaceutical assessments of inhalable therapeutics are most often predicted using in vitro-in vivo correlations of particle size to merely approximate deposition[4]. This technique does not allow for any spatial analysis to determine the effects of different airway geometries on regional distribution through the various lobes of the lung. Additionally, this testing lacks anatomically accurate lung geometries, which researchers have shown can have a significant impact on deposition profiles[5]. Some efforts have been made to incorporate patient-specific lung geometries into testing protocols through the addition of the upper airways; however, most of these approaches sample aerosol delivery to various generations of the lung rather than each lung lobe[6-8]. The following protocol presents a high-throughput method of generating patient-specific lung models with the capacity to quantify relative particle deposition in each of the five lobes of the lung[9].

Anatomically accurate model lungs are generated by 3D printing patient computed tomography (CT) scans. When used in conjunction with an easily assembled flow system, the relative flow rates through each of the model lung's lobes can be independently controlled and tailored to mimic those of different patient demographics and/or disease states. With this method, researchers can test the efficacy of potential therapeutic methods in a relevant lung geometry and correlate each method's performance with the progression of diseased morphology. Here, two device designs developed in our lab are tested for their ability to increase deposition in a desired lung lobe by controlling the location of aerosol release in the mouth or trachea. This protocol also has the potential to significantly impact the development of personalized procedures for patients by facilitating the rapid prediction of treatment efficacy in a model lung specific to that patient's CT scan data.

PROTOCOL:

1. Preparation of 3D printed experimental components

NOTE: All software used in the protocol are indicated in the **Table of Materials**. Additionally, the slicing software utilized is specific to the 3D printer listed in the **Table of Materials**; however, this protocol can be extended to a wide range of stereolithography (SLA) 3D printers.

1.1. Convert patient CT scans to 3D objects (.stl files).

NOTE: For a more detailed discussion of the geometrical features of the specific lung model used in these studies, refer to Feng et al.[5].

1.1.1. Render CT scans into a 3D object using CT scan software (see **Table of Materials**). Open the CT scan and create a mask on the airspace using the **Threshold** tool with a setting in the range of

-800 to -1000. Using the **3D Preview** tool, view the 3D rendering and export the object (**File | Export**) as an .stl file.

1.1.2. Importing the files into mesh editing software (see **Table of Materials**), remove any jagged features using the **Select** tool (**Sculpt | Brushes: "Shrink/Smooth" | Properties: Strength (50), Size (10), Depth(0)**). Smooth the surface **(Ctrl+A | Deform | Smooth | Smoothing (0.2), Smoothing Scale (1)**).

1.1.3. In mesh editing software, extend the wall of these objects by 2 mm (**Ctrl+A | Edit | Offset**), and allow the inner object to remain hollow such that only the wall remains. Slice the object (**Select | Edit | Plane Cut**) at the trachea to form an inlet and at generations 2 or 3 where the object branches off to each lobe to create outlets (**Figure 1A**).

NOTE: The thickness of 2 mm was chosen based on the acceptable feature sizes specified by the manufacturer of the 3D printer listed in the **Table of Materials**. This thickness can be adjusted based on the specifications of the 3D printer available if the interior geometry of the model is maintained.

1.2. Modify patient lung model outlet geometries to be compatible with previously designed lobe outlet cap components (**Figure 1B,C**) listed in the **Table of Materials**.

1.2.1. Import the 3D object, which replicates the CT scan on the inside, has a wall thickness of 2 mm, and is open at the inlet and outlets, into 3D modeling software (see **Table of Materials**) as a Solid Body (**Open | Mesh Files | Options | Solid Body**).

1.2.2. Create a plane based on a face at each of the outlets (**Insert | Reference Geometry | Plane**). Using the splicing tool, trace the inner wall and outer wall of the outlet in a sketch on the plane (**Sketch | Spline**).

1.2.3. Loft a cylinder (OD 18.5 mm, ID 12.5 mm, H 15.15 mm) to connect to the inner and outer wall of the model, thus extending the outlet to be uniform at each lobe (**Features | Lofted Boss/Base**). Add a notch around the edge of the outlet to match with the cap (**Features | Extruded Cut | Offset**).

NOTE: The cap (**Figure 1D**) is a hollow cylinder matching the dimensions of the outlets and having a shelf that interconnects with the notch of the model outlet. One end of the cap is blocked such that the ID is smaller than the rest of the part, this ensures a tight fit around the barbed tubing connection (**Figure 1E**). The barbed tubing connection is a barbed cone-shape such that the barbing fits through the opening of the cap, but the rest of the part does not, allowing the tubing connection to securely fit in the cap. Thus, the cap fits tightly around both the barbed tubing connection and the lung model (**Figure 1F,G**).

1.2.4. Modify the inlet of the lung model depending on the desired experimental conditions. The throat and glottal regions can be included to mimic a patient that can breathe on their own

(**Figure 1B**). Regions above the trachea can be removed using an extruded cut to mimic an intubated patient on ventilator support (**Features | Extruded Cut**) (**Figure 1C**).

1.3. Orient and support experimental components in slicing software provided by the 3D printer manufacturer.

1.3.1. Import 3D part files into 3D printer slicing software and choose the appropriate resin. Use a hard resin to print the lung models and barbed tubing connections, and a soft resin to print the caps.

NOTE: The resin used for printing the caps must have elastic properties to allow it to stretch over the lobe outlet and create an airtight seal.

1.3.2. Set the part orientation such that any "islands" and unvented volumes are minimized. The best orientation for the lung models is with the lobe outlets facing away from the print platform. Ensure both the barbed tubing connections and the caps have the wider portions facing the print platform.

NOTE: Individual slices can be viewed to check for the appearance of "islands," sections of the part that first appear in a slice without being connected to the main body of the part. The review function can be used to check for slices with unvented volumes, areas where uncured resin can get trapped inside the part during printing. Both "islands" and unvented volumes decrease print quality and could lead to print failure.

1.3.3. Viewing each slice individually, add supports to any remaining "islands" in the part as well as any areas with significant overhangs. Export and view the slices for the print to verify all areas are properly supported.

1.4. Print experimental components and complete post-processing as per manufacturer instructions.

NOTE: All post-processing steps described below are specific to the 3D printer listed in the **Table of Materials**. When utilizing alternate printers or materials, adjust these steps to reflect manufacturer instructions.

1.4.1. For parts printed in soft resin, wash with ≥99% purity isopropyl alcohol (IPA) to remove excess uncured resin and thermal cure in a convection oven for 8 h according to manufacturer specifications.

NOTE: Parts printed in soft resin can be very delicate immediately after printing, so special care should be taken during cleaning steps. Exposure to IPA should be kept below the material's solvent exposure limit to prevent part degradation.

1.4.2. For parts printed in hard resin, wash with IPA to remove excess uncured resin and cure in

a UV oven (365 nm light at 5-10 mW/cm^2) for 1 min per side.

NOTE: To evaluate the accuracy of the 3D printed replica, it is recommended to use µCT scanning of the printed part and CT scan software to compare, quantitatively, variations between the original 3D rendering and the 3D printed replica.

2. Assembly of tubing system for flow rate control

2.1. Screw 1/4” barbed tube fittings into the side of the manifold with 6 ports (**Figure 2A-6**) and a 3/8” barbed tube fitting into the remaining port.

2.2. Cut 1/4" tubing to desired lengths and insert into each end of the push-to-connect valves (**Figure 2A-5**). Attach each valve to one of the 1/4" fittings inserted in the manifold.

2.3. Connect a flow meter (**Figure 2A-4**) to the other end of each valve.

2.4. Position the tubing system on top of the wooden board such that the manifold’s single 3/8” fitting extends past the edge of the board. To secure in place, add two screws to the side of the wooden board and attach the manifold to the screws using wire.

2.5. Add four screws positioned around each of the valves and flow meters and use wire to secure each of them to the wooden board (**Figure 2E**).

2.6. With approximately 6” of 3/8” ID tubing, connect the manifold to an in-line 0.1 µm pore size vacuum grade filter. Connect the other end of the filter to the flow controller using another 6” of 3/8” ID tubing

NOTE: The tubing system only needs to be assembled once.

3. Assembly of lobe outlet caps with patient lung model

NOTE: This portion of the protocol must be completed prior to every experimental run.

3.1. Insert barbed tubing connection into the cap with nozzle protruding through the opening in the cap base. First, insert one end of the oval barbed tubing connection base into the cap. Then, carefully stretch the flexible cap over the other end of the oval base, taking special care not to crack the thin base.

NOTE: Newly printed caps may be stiffer than desired and can be stretched out by running two fingers along the cap interior.

3.2. Cut 10 µm filter paper such that it is slightly larger than the outlet area. Fold the filter paper over the lobe outlet and hold in place with one hand.

3.3. With the other hand, use tweezers to stretch the cap with barbed tubing connection over the outlet. Press the cap down until the cap's notch matches up with the corresponding notch on the lobe outlet (**Figure 2C**).

NOTE: Ripping the filter paper in this step can invalidate results, so special care should be taken to avoid excessive force when pressing the cap onto the outlet.

3.4. Repeat for all remaining lobe outlets (**Figure 2D**).

4. Generation of clinically relevant air flow profile

NOTE: This portion of the protocol must be completed prior to every experimental run.

4.1. Connect each lung model lobe outlet to the tubing of the corresponding flow meter and valve, taking care not to apply too much lateral pressure to the barbed tubing connection. Attach the electronic flow meter to the lung model mouth inlet to measure total air flow rate to the lung model.

4.2. Turn on the flow controller (**Figure 2A-7**) and vacuum pump (**Figure 2A-8**). Select the "**test setup**" setting on the flow controller and slowly increase the flow rate until the electronic flow meter displays the desired total flow rate.

4.3. Using the valves (**Figure 2E-5**), adjust the flow rate through each of the five lung lobes: Right Upper (RU), Right Middle (RM), Right Lower (RL), Left Upper (LU), and Left Lower (LL). Once the lobe flow rates shown on the flow meters (**Figure 2E-4**) are steady at the desired value, check the overall flow rate again on the electronic flow meter to verify that there are no leaks in the system.

4.3.1. If there is a discrepancy in the total flow rate, lower the flow rate with the flow controller, set all valves to the fully open configuration, and repeat steps 4.2 and 4.3.

NOTE: Results presented here were obtained using air flow profiles based on data reported by Sul et al.[10] These lobar flow fractions were calculated using thin-slice computed tomography images of patient lungs at full inspiration and expiration, comparing the relative changes in the volume of each lung lobe. Results are presented for two distinct flow conditions, both at an overall inlet flow rate of 1 L/min. The healthy lung lobe outlet flow profile is distributed to each outlet by the following percentage of the inlet flow: LL-23.7%, LU-23.7%, RL-18.7%, RM-14.0%, RU-20.3%. The COPD lobe outlet flow profile is distributed between each outlet by the following percentage of the inlet flow: LL-10.0%, LU-29.0%, RL-13.0%, RM-5.0%, RU-43.0%[9,10].

4.4. Exit the "**test setup**" function of the flow controller but leave the vacuum pump on.

NOTE: Turning the vacuum pump off in between setting the flow rates and performing the deposition experiment can lead to inaccuracies in the flow profile generated. It is recommended to leave the vacuum pump on once desired flow rates are set to complete the aerosol deposition

testing.

5. Delivery of aerosol to the lung model

NOTE: Experiments must be performed in a fume hood with the sash closed to minimize exposure to any aerosols generated by the nebulizer.

5.1. Fill nebulizer with solution of desired fluorescent particles (**Figure 2A-1**) and connect to the lung model inlet (**Figure 2B**).

NOTE: Results presented here were obtained using 30 mL a 1:10 dilution of 1 µm fluorescent polystyrene particles in methanol.

5.1.1. To validate the experimental setup, connect the nebulizer directly to the lung model inlet without any targeting device.

5.1.2. To measure the efficacy of a targeting device, connect the nebulizer to the device and insert the device into the lung model.

5.2. Connect the compressed air line to the nebulizer and close the fume hood sash as much as possible.

5.3. Set the flow controller to run for one 10 s trial. Before pressing start, open the compressed air valve slightly to begin generating an aerosol within the nebulizer.

5.4. Press start on the flow controller and immediately open the compressed air valve fully. Once the flow controller reaches about 9 s, begin to close the compressed air valve.

5.5. Once the compressed air valve is fully closed, disconnect the nebulizer from the compressed air line, fully close the fume hood sash, shut off the vacuum pump, and let any aerosols clear from the fume hood for about 10 min.

NOTE: It is important to shut the vacuum pump off after completing a run to prevent a vacuum from building up within the tubing system.

5.6. After waiting for a sufficient amount of time, disconnect the lung model from the tubing system, taking special care not to crack the barbed tubing connections.

5.7. Remove the lobe outlet caps by running a pair of tweezers under the edge of the cap and gently lifting it off the lung model.

5.8. Remove the filter paper from the cap and place it into a 24 well plate with the side onto which particles deposited being on the bottom facing the well of the plate. Repeat for the remaining outlets and label the well corresponding to each lobe.

NOTE: To prevent any residual particle deposition from impacting subsequent experiments, it is important to rinse both the lung model and cap components with IPA or appropriate solvent in between runs. This can be collected and included in the analysis as desired. Additionally, a log is kept to ensure all replicas used have been minimally exposed to IPA to maintain part integrity and visual part inspection is recommended prior to use.

6. Outlet filter paper imaging

6.1. Place the well plate into the digital fluorescence microscope and set the microscope to 4x magnification and the appropriate fluorescence channel.

6.2. Visually identify which lobe's filter paper has the highest amount of particle deposition and use the "**Auto Expose**" function. Take note of the resulting exposure and integration time values.

6.3. Apply this exposure to all the filters for the run and assess whether the setting produces a satisfactory image for all high deposition areas of the filters.

NOTE: Focus settings can be changed from filter to filter; however, all the filters for a given run must be analyzed at the same exposure settings. It is only possible to have one frame of focus at a time, so bends or tears in the filter paper may prevent all the deposited particles in the view from being in focus. This can be avoided by ensuring the filter paper is flat against the bottom of the well plate.

6.4. Take at least three images of each lobe's filter paper at random locations and save as .tiff files.

7. Quantification of particle deposition

7.1. Import all the filter paper pictures for a given run into an ImageJ session.

7.2. Change each image's type to 8-bit by selecting **Image | Type | 8-bit**.

7.3. Open the picture with the highest fluorescence and select **Image | Adjust | Threshold** to open a threshold window. Adjust the threshold values to minimize background signal from the filter paper and clearly define the edges of particles. See **Figure 3** for depictions of good-quality and poor-quality thresholding.

NOTE: For filters with high levels of deposition, a "corona" of fluorescence, caused by the diffraction of light by the filter paper fibers, may be observed around large groupings of particles. When thresholding these images, a range that is too large displays small dots or "feather-like" shapes around these groupings, as observed in the "poor" threshold images in **Figure 3**. This can be improved by gradually increasing the lower limit of the threshold until the signal from the filter paper fibers is minimized without obscuring the signal from the particles themselves.

7.4. Propagate the threshold settings for the highest fluorescence image to all other images.

7.5. Quantify the number of particles and the total fluorescent area by selecting **Analyze | Analyze Particles**.

NOTE: Data sets are compared using Sidak's Multiple Comparisons Test and a two-way ANOVA. Additionally, deposition in just the lobe of interest is compared using a Student T-test assuming equal variance.

REPRESENTATIVE RESULTS:

Particles in this size range (1-5 µm) and flow conditions (1-10 L/min) follow the fluid stream lines based on both their theoretical Stokes number and in vivo data; therefore, in the absence of a targeted delivery device, particles released into the lung model are expected to deposit according to the percentage of total airflow diverted to each lobe. The relative amounts of particle delivery to each lobe can then be compared to clinical lobe flow rate data obtained through analyzing patient-specific high-resolution computed tomography (HRCT) scans[10]. A validated experimental set-up will yield a non-targeted particle deposition profile that has no statistically significant difference from the clinical air flow profile. Validation data is presented for two distinct flow conditions: 1 L/min in a healthy lung (**Figure 4A**) and 1 L/min in a lung affected by COPD (**Figure 4B**). Under both these conditions, the experimentally determined deposition profile was not statistically different from the clinical data, demonstrating that the set-up accurately mimics the distribution of air flow to each of the lung lobes. These baseline deposition profiles served as the control against which targeted particle deposition profiles are compared.

To illustrate this protocol's ability to quantify changes in regional pulmonary deposition, data were included for the testing of two different targeting devices: a modified endotracheal (ET) tube (**Figure 5B**) and a concentric cylinder device (**Figure 5E**). Both these devices featured a 2 mm ID outlet with tunable location for targeted particle release. The modified ET tube was assessed with the intubated lung model for its ability to target particle deposition to both the Left Lower (LL) Lobe and Right Lower (RL) Lobe. Compared to the non-targeted particle deposition profile, this device generated a nearly four-fold increase in LL Lobe delivery (T-test p=0.004, n=3) in addition to diverting over 96% of delivered particles to the Left Lung (T-test p=0.0001, n=3) (**Figure 5A**). Altering the release location setting to target the RL Lobe, this device generated more than doubles particle delivery to the RL Lobe (T-test p=0.02, n=3) and diverted 94% of delivered particles to the Right Lung (T-test p=0.0005, n=3) (**Figure 5C**). This indicates that the device is highly successful in producing the intended deposition profile modulation. The concentric cylinder device was tested in the full lung model with an intended target of the Left Upper (LU) Lobe. Compared to the non-targeted particle deposition profile, this device caused a nearly three-fold increase in LU Lobe delivery (T-test p=0.0003, n=3) in addition to diverting over 87% of delivered particles to the Left Lung (T-test p=0.002, n=3) (**Figure 5D**). Targeting efficiency can also be observed qualitatively by comparing the images of the target lobe filter to the other outlet filters. As depicted in **Figure 3**, the most effective targeting method will yield high particle deposition at the intended lobe of interest and low deposition at the remaining lobe outlets. For

further demonstrations of the capabilities of this protocol, please see the experiments performed by Kolewe et al[9].

FIGURE AND TABLE LEGENDS:

Figure 1: 3D printed experimental components. (**A**) Patient CT scan converted into 3D part file using CT scan and mesh editing software. (**B**) Lung model with lobe outlet modifications made in mesh editing and 3D modeling software. (**C**) Lung model with inlet modified in 3D modeling software to reflect an intubated patient. (**D**) Barbed tubing connection and (**E**) cap designed in 3D modeling software. (**F**) Cross-section of 3D model depicting the interlocking nature of the lung model outlets with the cap and barbed tubing connection. **(G)** Exploded view of lung model outlet cap assembly.

Figure 2: Assembly of experimental setup. (**A**) Schematic of experimental setup including (1) nebulizer, (2) lung model, (3) outlet caps, (4) flow meters, (5) valves, (6) manifold, (7) flow controller and (8) a vacuum pump. (**B**) Fully assembled setup. (**C**) Close-up of lobe outlet with assembled cap. (**D**) Lung model with all caps added. (**E**) Close-up of tubing network for setting lobe outlet flow rates.

Figure 3: Filter paper image processing. The raw images presented were collected during an experiment to target the left lung using 1 µm fluorescent polystyrene particles at 1 L/min under a healthy breathing profile. The "high" and "low" deposition images depict the LL and RU Lobe filters, respectively. The "good" threshold, applied with a range of 43 to 255, maintains defined edges between individual particles and avoids detection of filter paper fibers. The "poor" threshold, applied with a range of 17 to 255, obscures individual particle borders and overestimates the fluorescent area of the filter.

Figure 4: Experimental setup validation. (**A**) Validation results for healthy patients and (**B**) a COPD patient at 1 L/min. All data presented are mean ± SD with three replicates (excepting clinical COPD data, where only one patient was reported). Clinical reference data for healthy and COPD patients were obtained from Sul, et al[10]. Data sets were compared using Sidak's Multiple Comparisons Test, and all differences are not significant.

Figure 5: Example data for targeting experiments. (**A**) Left Lower Lobe and (**C**) Right Lower Lobe targeting achieved using (**B**) a modified ET tube delivery system. (**D**) Left Upper Lobe targeting achieved using (**E**) a concentric tube delivery system. For all three data sets, the inner ring represents the non-targeted deposition profile obtained during setup validation, and the outer ring represents the deposition profile produced with the addition of the indicated targeting device. Means of three replicates for each setup are shown. Data sets were compared using Sidak's Multiple Comparisons Test and a Student T-test assuming equal variance. All three setups produced a significant increase in delivery to the lobe of interest: LL Lobe (T-test $p=0.004$, $n=3$), RL Lobe (T-test $p=0.02$, $n=3$), and LU Lobe (T-test $p=0.0003$, $n=3$).

DISCUSSION:

The current state-of-the-art device for pulmonary pharmaceutical testing of a complete inhalation dose is the Next Generator Impactor (NGI), which measures the aerodynamic diameter of an aerosol[4]. This sizing data is then used to predict the lung generation at which the aerosol will deposit based on a correlation developed for a healthy adult male[11]. Unfortunately, this method is limited in its ability to assess differences in regional lung deposition, determine the effects of disease conditions on pharmaceutical delivery, and predict deposition profiles for various age groups, races, and genders[12-14]. The protocol outlined here has the capacity to fulfill these testing needs by allowing researchers to generate tunable, anatomically accurate lung models with the ability to quantify relative deposition at the lobe level, based on fluid flow behavior previously demonstrated in computational models[3,5,15]. Using this method, pharmaceutical dosage and delivery can be better assessed for pediatric and diseased lung geometries prior to entering clinical trials.

As shown in **Figures 4** and **Figure 5**, lobe-level deposition can be accurately and rapidly measured for both targeted and non-targeted inhalation aerosols. In the absence of a targeting device, particles in this size range (1-5 µm) and flow conditions (1-10 L/min) follow the fluid streamlines and total airflow profile diverted to each lobe (**Figure 4**). Notably, various inhaler devices and ET tube attachments can be developed to concentrate inhaled medicines to controlled lobe locations. As described in our recent work and those of others, many features of the inhaler device, flow profile, and airway geometry contribute to targeted deposition behavior[2,3,9,16]. In general, efficient regional targeting as demonstrated by our unique in vitro models requires a narrow aerosol size distribution and low inhalation flow rates to avoid airway turbulence specifically found within the trachea. Inclusion of the full upper airway within our in vitro model allows for accurate recreation these airflow patterns that are known to influence downstream lobe-level distribution[9]. Because of these complex flows, recent work has demonstrated increased targeting from below the glottis[9]. Our results in **Figure 5** specifically highlight the benefit of using an ET tube adaptor to regionally target individual lobes from release below the glottis, with efficient lobe-specific targeting shown for lobes of both the right and left lungs at efficiencies ranging between 62-74% of the total dose. This represents an increase over previously experimentally reported mouth-release regional targeting efficiencies and is an important avenue for clinical implementation of this approach[9]. Importantly, the protocol allows for experimental lobe distribution measurements of a complete pharmaceutical dosage from a wide range of potential regional targeting devices beyond those demonstrated here.

With only a CT scan, a patient-specific lung model can be quickly 3D printed to test a potential therapeutic delivery method. This protocol will not only provide an experimental lab-scale approach to support design of new inhaler devices, but also create opportunity for on-demand personalized inhalation devices in clinical practice. The hard resin used in this protocol costs ~$0.12/mL; therefore, hospitals with existing 3D printing infrastructure could print a lung model for as little as $15 in materials[17] and assemble a personalized airway in under a day. Notably, printing times and material costs in additive manufacturing continue to decrease rapidly, increasing the overall feasibility of this approach. Our experimental set-up can be easily modified to reflect number of airflow conditions through utilizing a different lung model or air flow distribution setting, following the experimental validation shown in **Figure 4**. Differences in lung

flow profiles and geometries due to characteristics such as age, race, and sex are well documented in literature and can be readily incorporated into our modelling approach[18-20]. Specifically, geometric variations in the larynx, pharynx, and trachea of lung models can have a significant impact on airflow and subsequent regional deposition patterns[15,21,22], which this protocol is well-equipped to detect. Thus, incorporation of this personalized modelling approach is expected to have significant impact on the development of customized inhalation therapeutics.

Here, the lobe flow rates were altered to reflect those of a COPD disease state characterized by decreased air flow to the lower lobes (**Figure 4B**), but COPD patient-derived CT scans could also be used to more accurately mimic the diseased lung architecture and possible obstructions[23]. With a library of patient lung models and flow profiles, the effects of disease progression on delivery efficiency can be investigated. There is a wide range of open source scans available from organizations, such as the National Institutes of Health (NIH) and the Cancer Imaging Archive (TCIA)[24]. While these models currently can only replicate patient geometry up to the second or third generation to adequately measure lobe-level distribution, work is ongoing to develop modifications that can incorporate the lower airways for more detailed analysis. This protocol can also incorporate clinically relevant drug delivery devices such as an ET tube as depicted in **Figure 5B**. Researchers can evaluate multiple delivery devices to reveal characteristics that may increase or decrease treatment efficiency. For example, targeting effectiveness is reduced when attempted in the full lung model as opposed to the intubated lung model (**Figure 5**). This difference indicates that bypassing the glottal region avoids areas of turbulent mixing that diminish targeting ability.

This protocol is limited by its inability to accurately mimic the biological air-liquid interface. As a result, aerosols that normally deposit by inertial impaction may instead bounce off the rigid walls of the lung model[25]. To ameliorate this, future directions include exploring surface modifications and coatings to mimic the mucosal layer of the lung epithelium. Coatings such as silicon oil and glycerin have been investigated for the prevention of particle bounce in an NGI and could easily be incorporated onto the 3D printed lung models[26]. Other techniques such as bioprinting and culturing cells on 3D printed models are being investigated for their ability to incorporate a cellular response into the protocol[27]. Additionally, this protocol uses equipment optimized for flow rates of 1-15 L/min; in the future, higher flow rates of 30-60 L/min, the normal range of peak inspiratory flow rates, could be used by switching out the control valves and flow meters for ones appropriate for the desired flow rate range[28,29]. With the flow controller model used, the system is only capable of modeling inspiration rather than a full cyclical breathing cycle. Incorporation of transient breathing patterns through the use of a ventilator or more complex flow system would likely improve the accuracy of experimental results with respect to particle deposition efficiency[30]. Lastly, deposition experiments have only been performed with monodisperse fluorescent polystyrene spheres ranging in size from 1-5 µm. Deposition quantification relies on aerosol fluorescence, so the use of this protocol with non-fluorescent aerosols may require the incorporation of a fluorescent label such as fluorescein isothiocyanate (FITC) for analysis[31]. However, additional analytical techniques could be applied to analyze the filter depending on the aerosol composition, such as high-performance liquid chromatography (HPLC) and or mass spectrometry.

Our protocol demonstrates the first in vitro experimental setup with the ability to quantify lobular pulmonary deposition in a patient-specific lung geometry. Achieving controlled lobe-level distribution is expected to increase therapeutic efficacy of inhalation therapeutics, which will only be achieved through advances in in vitro whole-dose measurements. With the growing interest in personalized medicine, this protocol has the potential to spur the development of new targeted lung therapies by allowing for more accurate predictions of potential treatment efficacy.

ACKNOWLEDGMENTS:

The authors thank Professor Yu Feng, Dr. Jenna Briddell, Ian Woodward, and Lucas Attia for their helpful discussions.

DISCLOSURES:

The authors have nothing to disclose.

REFERENCES:

1. Goel, A., Baboota, S., Sahni, J. K., Ali, J. Exploring targeted pulmonary delivery for treatment of lung cancer. *International Journal of Pharmaceutical Investigation.* **3** (1), 8-14 (2013).
2. Kleinstreuer, C., Zhang, Z., Li, Z., Roberts, W. L., Rojas, C. A new methodology for targeting drug-aerosols in the human respiratory system. *International Journal of Heat and Mass Transfer.* **51** (23), 5578-5589 (2008).
3. Feng, Y., Chen, X., Yang, M. An In Silico Investigation of a Lobe-Specific Targeted Pulmonary Drug Delivery Method. *Design of Medical Devices Conference.* (2018)
4. Marple, V. A. et al. Next generation pharmaceutical impactor (a new impactor for pharmaceutical inhaler testing). Part I: Design. *Journal of Aerosol Medicine.* **16** (3), 283-299 (2003).
5. Feng, Y., Zhao, J., Chen, X., Lin, J. An In Silico Subject-Variability Study of Upper Airway Morphological Influence on the Airflow Regime in a Tracheobronchial Tree. *Bioengineering.* **4** (4), 90 (2017).
6. Huynh, B. K. et al. The Development and Validation of an In Vitro Airway Model to Assess Realistic Airway Deposition and Drug Permeation Behavior of Orally Inhaled Products Across Synthetic Membranes. *Journal of Aerosol Medicine and Pulmonary Drug Delivery.* **31** (2), 103-108, (2018).
7. Lizal, F., Elcner, J., Hopke, P. K., Jedelsky, J., Jicha, M. Development of a realistic human airway model. *Proceedings of the Institution of Mechanical Engineers, Part H: Journal of Engineering in Medicine.* **226** (3), 197-207 (2011).
8. Wei, X., Hindle, M., Delvadia, R. R., Byron, P. R. In Vitro Tests for Aerosol Deposition. V: Using Realistic Testing to Estimate Variations in Aerosol Properties at the Trachea. *Journal of Aerosol Medicine and Pulmonary Drug Delivery.* **30** (5), 339-348 (2017).
9. Kolewe, E. L., Feng, Y., Fromen, C. A. Realizing Lobe-Specific Aerosol Targeting in a 3D-Printed In Vitro Lung Model. *Journal of Aerosol Medicine and Pulmonary Drug Delivery.* 10.1089/jamp.2019.1564, (2020).

10. Sul, B. et al. Assessing Airflow Sensitivity to Healthy and Diseased Lung Conditions in a Computational Fluid Dynamics Model Validated In Vitro. *Journal of Biomechanical Engineering.* **140** (5), (2018).
11. Martonen, T. B., Katz, I. Deposition Patterns of Polydisperse Aerosols Within Human Lungs. *Journal of Aerosol Medicine.* **6** (4), 251-274 (1993).
12. Nahar, K. et al. In vitro, in vivo and ex vivo models for studying particle deposition and drug absorption of inhaled pharmaceuticals. *European Journal of Pharmaceutical Sciences.* **49** (5), 805-818 (2013).
13. Nichols, S. C. et al. A Multi-laboratory in Vitro Study to Compare Data from Abbreviated and Pharmacopeial Impactor Measurements for Orally Inhaled Products: a Report of the European Aerosol Group (EPAG). *AAPS PharmSciTech.* **17** (6), 1383-1392 (2016).
14. Yoshida, H., Kuwana, A., Shibata, H., Izutsu, K. I., Goda, Y. Comparison of Aerodynamic Particle Size Distribution Between a Next Generation Impactor and a Cascade Impactor at a Range of Flow Rates. *AAPS PharmSciTech.* **18** (3), 646-653 (2017).
15. Feng, Y. et al. An in silico inter-subject variability study of extra-thoracic morphology effects on inhaled particle transport and deposition. *Journal of Aerosol Science.* **123** 185-207 (2018).
16. Kleinstreuer, C., Seelecke, S. Inhaler system for targeted maximum drug-aerosol delivery. United States patent (2005).
17. Pietila, T. *How Medical 3D Printing is Gaining Ground in Top Hospitals*, <https://www.materialise.com/en/blog/3D-printing-hospitals> (2019).
18. Weber, P. W., Price, O. T., McClellan, G. E. Demographic Variability of Inhalation Mechanics: A Review. Defense Threat Reduction Agency (2016).
19. Jiang, Y.-Y., Xu, X., Su, H.-L., Liu, D.-X. Gender-related difference in the upper airway dimensions and hyoid bone position in Chinese Han children and adolescents aged 6–18 years using cone beam computed tomography. *Acta Odontologica Scandinavica.* **73** (5), 391-400 (2015).
20. Martin, S. E., Mathur, R., Marshall, I., Douglas, N. J. The effect of age, sex, obesity and posture on upper airway size. *European Respiratory Journal.* **10** (9), 2087 (1997).
21. Xi, J., Longest, P. W., Martonen, T. B. Effects of the laryngeal jet on nano- and microparticle transport and deposition in an approximate model of the upper tracheobronchial airways. *Journal of Applied Physiology.* **104** (6), 1761-1777 (2008).
22. Zhao, J., Feng, Y., Fromen, C. A. Glottis motion effects on the particle transport and deposition in a subject-specific mouth-to-trachea model: A CFPD study. *Computers in Biology and Medicine.* **116**, 103532 (2020).
23. Kim, S. S. et al. Chronic obstructive pulmonary disease: lobe-based visual assessment of volumetric CT by Using standard images--comparison with quantitative CT and pulmonary function test in the COPDGene study. *Radiology.* **266** (2), 626-635 (2013).
24. *The Cancer Imaging Archive*, <https://www.cancerimagingarchive.net/> (2020).
25. Li, A., Ahmadi, G. Computer Simulation of Deposition of Aerosols in a Turbulent Channel Flow with Rough Walls. *Aerosol Science and Technology.* **18** (1), 11-24 (1993).
26. Khalili, S. F., Ghanbarzadeh, S., Nokhodchi, A., Hamishehkar, H. The effect of different coating materials on the prevention of powder bounce in the next generation impactor. *Research in Pharmaceutical Sciences.* **13** (3), 283-287 (2018).

27. Galliger, Z., Vogt, C. D., Panoskaltsis-Mortari, A. 3D bioprinting for lungs and hollow organs. *Translational Research.* **211**, 19-34 (2019).
28. Schwarz, K., Biller, H., Windt, H., Koch, W., Hohlfeld, J. M. Characterization of exhaled particles from the healthy human lung--a systematic analysis in relation to pulmonary function variables. *Journal of Aerosol Medicine and Pulmonary Drug Delivery.* **23** (6), 371-379 (2010).
29. Patton, J. S., Byron, P. R. Inhaling medicines: delivering drugs to the body through the lungs. *Nature Reviews Drug Discovery.* **6** (1), 67-74 (2007).
30. Zhang, Z., Kleinstreuer, C., Kim, C. S. Cyclic micron-size particle inhalation and deposition in a triple bifurcation lung airway model. *Journal of Aerosol Science.* **33** (2), 257-281 (2002).
31. Ju, Y. et al. Engineering of Nebulized Metal–Phenolic Capsules for Controlled Pulmonary Deposition. *Advanced Science.* **7** (6), 1902650 (2020).

Figure 1

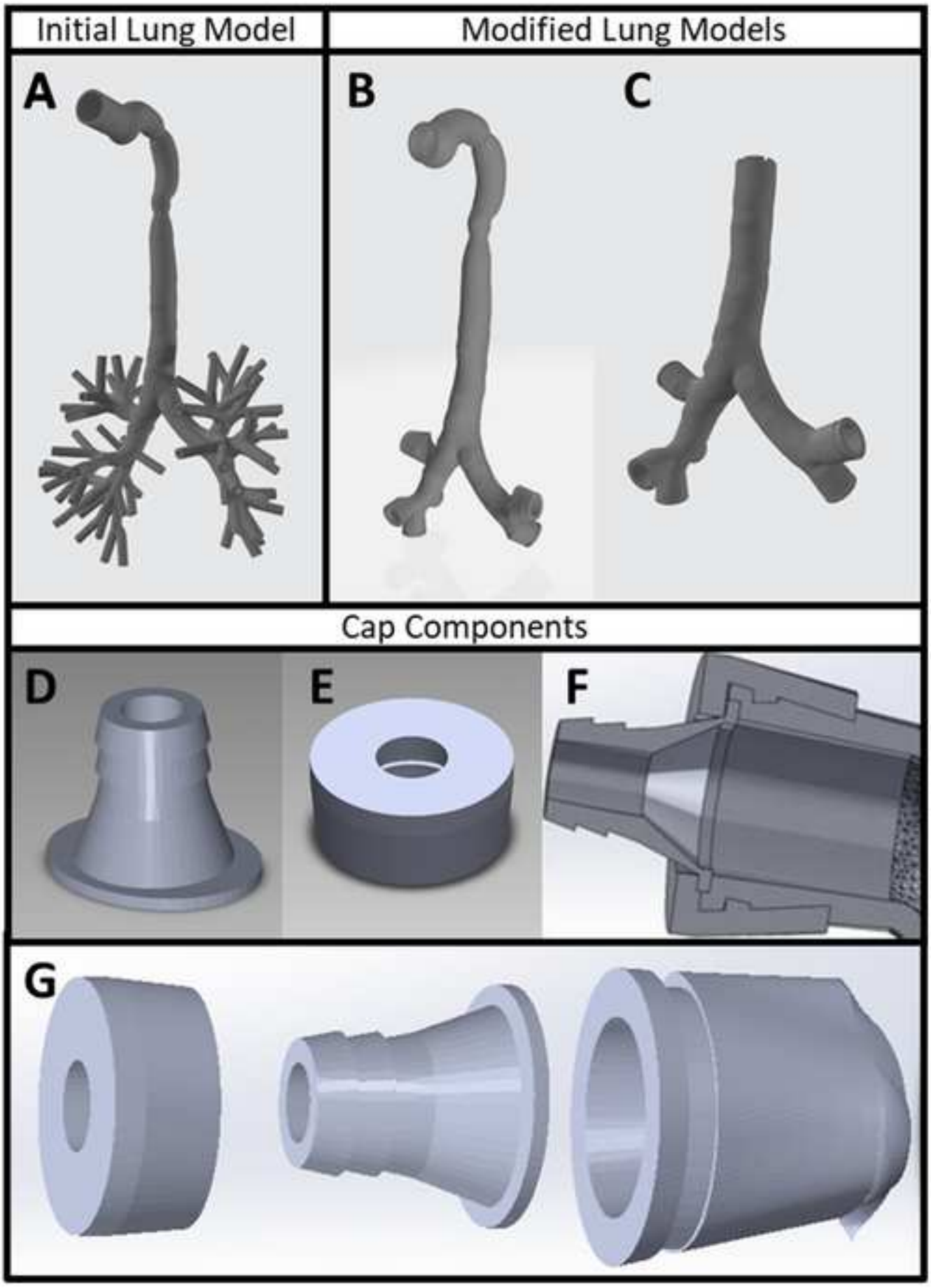

Figure 2

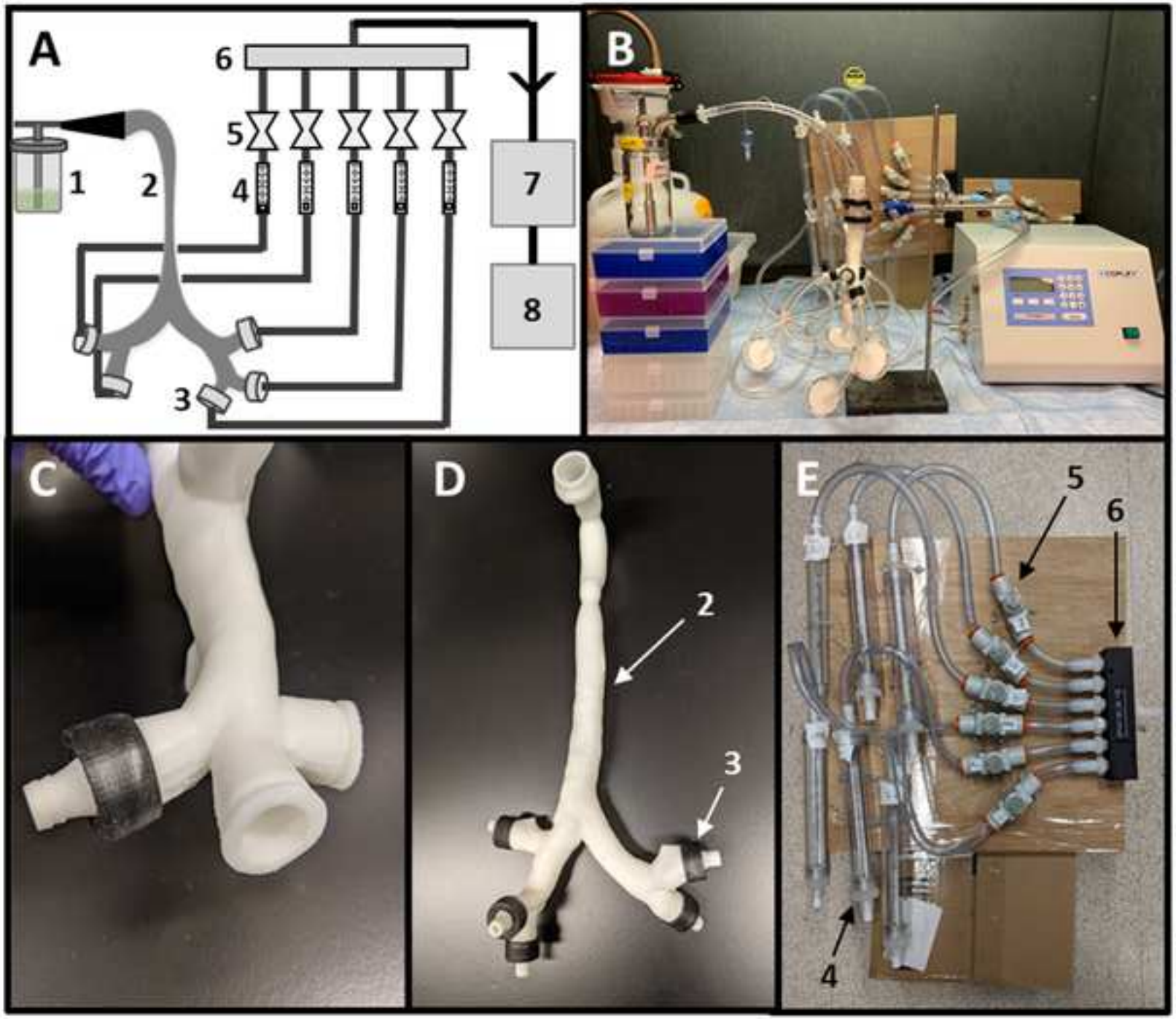

Figure 3

Click here to access/download;Figure;Figure3.tif

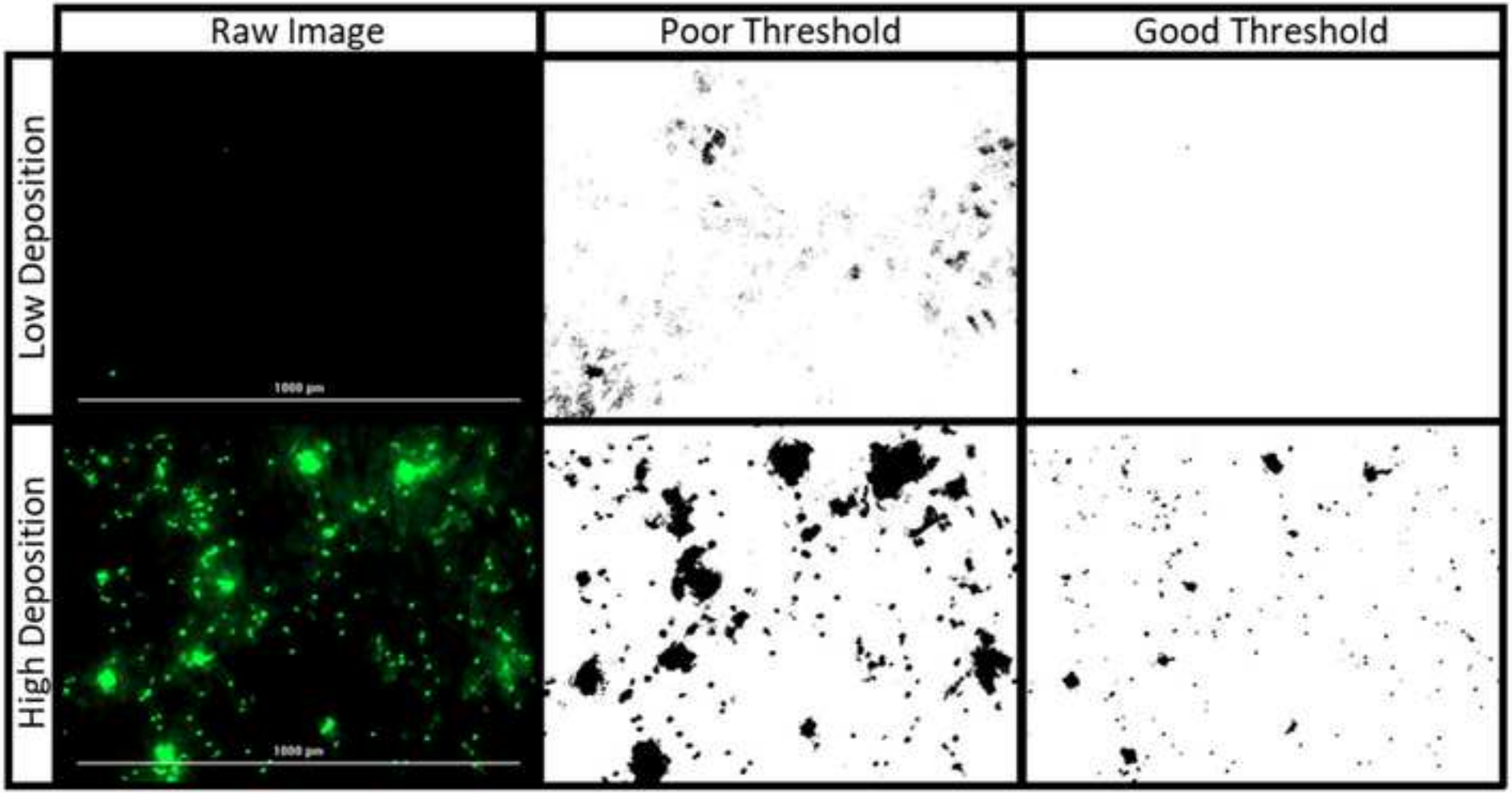

Figure 4

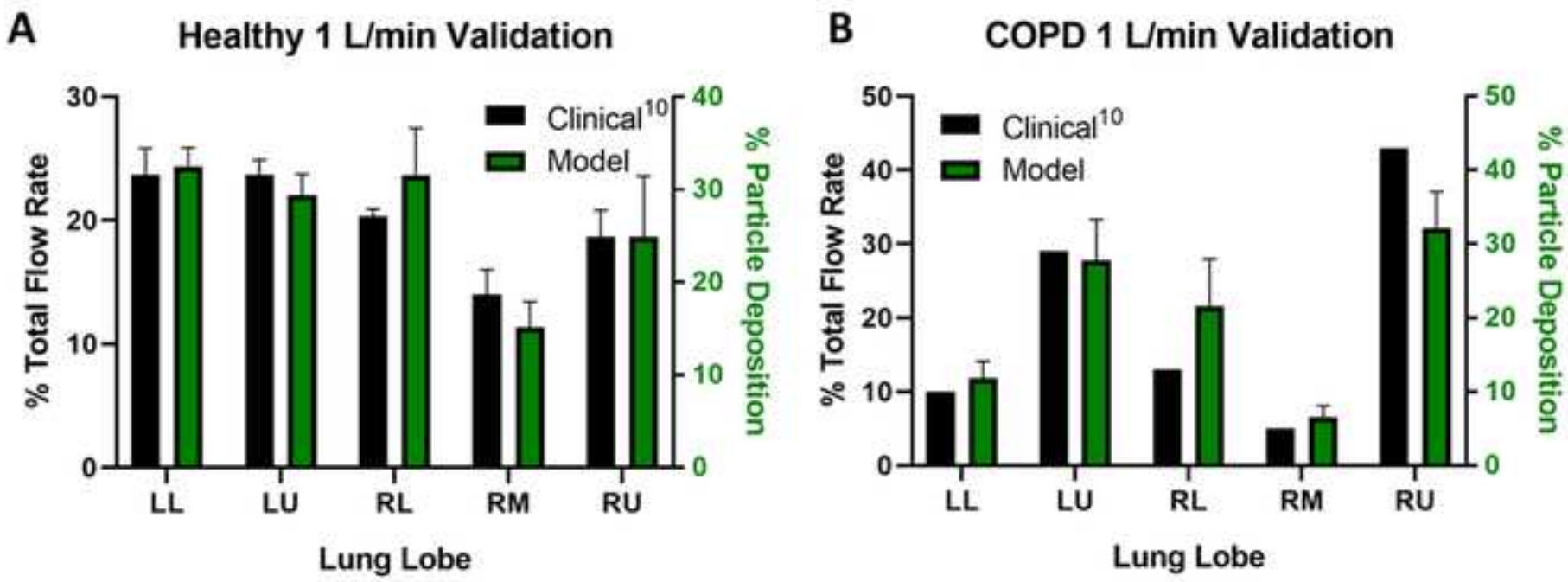

Figure 5

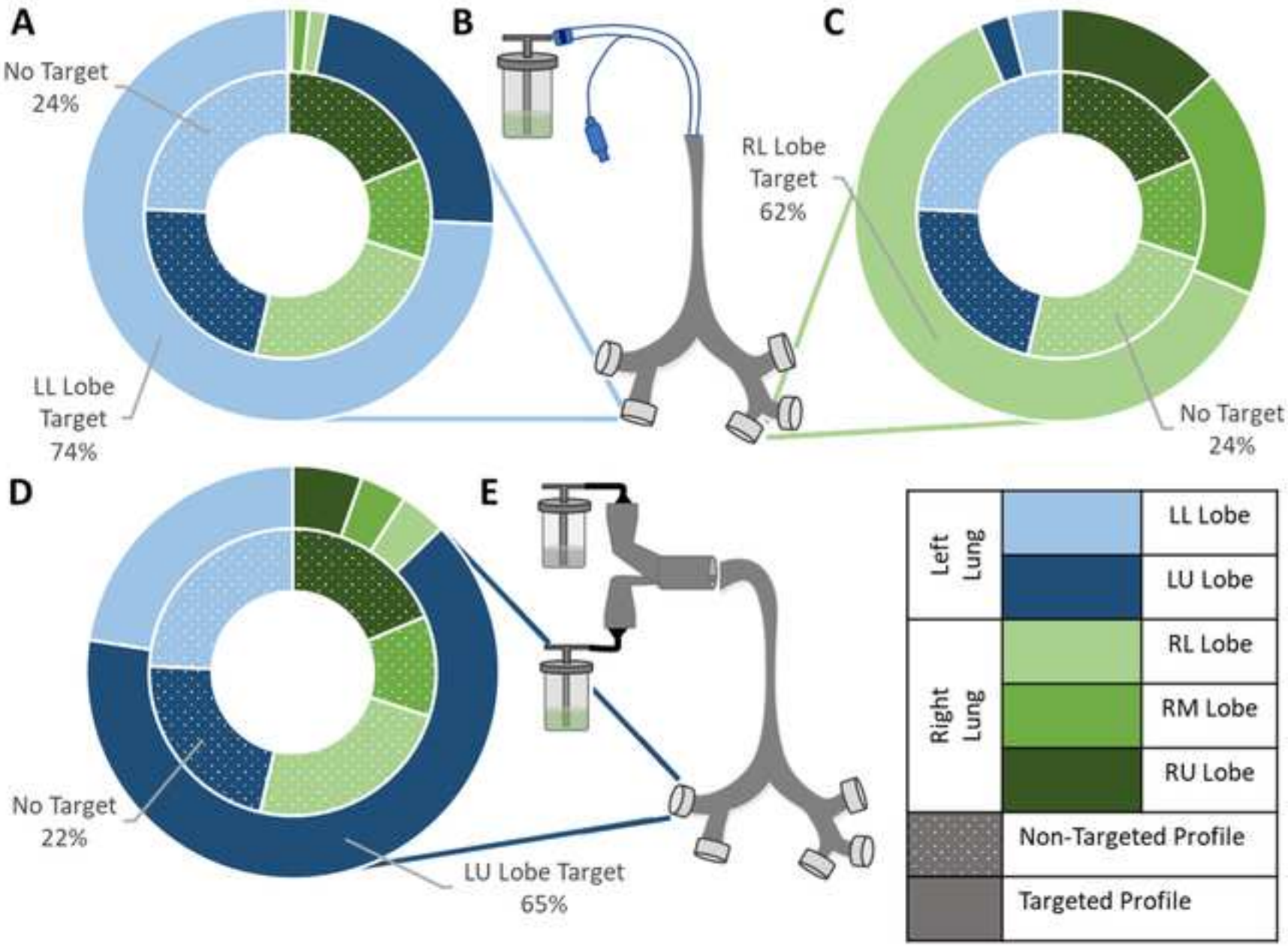

Table of Materials

Click here to access/download;Table of Materials;20200709_JoVE_Table_of_Materials_Alphabetical.xlsx

Name of Material/Equipment	Company	Catalog Number
1/4" Plastic Barbed Tube Fitting	McMaster Carr	5372K111
10 um Filter Paper	Fisher	1093-110
1um Fluorescent Polystyrene Particles	Polysciences	15702-10
1um Non-Fluorescent Polystyrene Particles	Polysciences	8226
2-Propanol	Fisher	A516-4
3/8" Plastic Barbed Tube Fitting	McMaster Carr	5372K117
Air Flow Meter (1 - 280 mL/min)	McMaster Carr	41695K32
Carbon M1 3D Printer	Carbon 3D	
Collison Jet Nebulizer	CH Technologies	ARGCNB0008 (CN-25)
Convection Oven	Yamato	DKN602
Copley Critical Flow Controller TPK2000 Reve 120V	MSP Corp	0001-01-9810
Copley High Capacity Pump Model HCP5	MSP Corp	0001-01-9982
Cytation	BioTek	CYT5MPV
EPU40 Resin	Carbon 3D	
Filter for vacuum pump	Whatman	6722-5000
Flow Meter Model DFM 2000	MSP Corp	0001-01-8764
ImageJ Software	ImageJ	
Inline Air Flow Control Valve (Push-to-Connect)	McMaster Carr	62005K333
Inline Filter Devices	Whatman	WHA67225000
Marine-Grade Plywood Sheet	McMaster Carr	62005K333
Materialise Mimics Software	Materialise	
Meshmixer Software	Autodesk	
Methanol	Fisher	A454-4
Opticure LED Cube	APM Technica	102843
PR25 Resin	Carbon 3D	
PVC Tube for Chemicals	McMaster Carr	5231K161
Screws		
SolidWorks Software	Dassault Systèmes SolidWorks Corporation	
Straight Flow Rectangular Manifold	McMaster Carr	1125T31
Tubing to Flow Controller	McMaster Carr	5233K65

Wire

Comments/Description

Referred to in protocol as "IPA"

Referred to in protocol as "flow meter"
https://www.carbon3d.com/, Associated software referred to in protocol as "slicing software"
6 Jet MRE style horizontal collision with glass jar, Referred to in protocol as "nebulizer", http://chtechusa.com/Manuals/MRE_Collisc

Referred to in protocol as "flow controller"
Referred to in protocol as "vacuum pump"
Multifunctional Spectrophotometer/Fluorescent imager equiped with 4x/20x/40x objectives and DAPI/GFP/TexasRed laser/filter cub
https://www.carbon3d.com/materials/epu-elastomeric-polyurethane/, Referred to in protocol as "soft resin"

Referred to in protocol as "electronic flow meter"
https://imagej.nih.gov/ij/download.html

Referred to in protocol as "valve"

Referred to in protocol as "wooden board"
https://www.materialise.com/en/medical/mimics-innovation-suite, Referred to in protocol as "CT scan software"
http://www.meshmixer.com/, Referred to in protocol as "mesh editing software"

Referred to in protocol as "UV oven"
https://www.carbon3d.com/materials/uma-urethanemethacrylate, /Referred to in protocol as "hard resin"
1/4" ID

https://www.solidworks.com/, Referred to in protocol as "3D modeling software"

3/8" ID

ɔn_Manual.pdf

es

Reviewer Responses:

We greatly thank both of the reviewers and the editor for their suggestions and their critical evaluation of this manuscript; your comments were hugely helpful in improving the manuscript overall. We have made a number of changes to our manuscript in response to these valuable recommendations, as detailed in a point by point response below. For convenience, new additions to the text are included in blue font, corresponding to the track changes sections in the attached manuscript. Page and Line reference numbers indicate locations in the tracked-changes version of the document.

Editorial Comments

***Protocol Detail**: Please add more specific details (e.g. button clicks for software actions, numerical values for settings, etc) to your protocol steps.*

1. *1.1, 1.2: mention button clicks and menu selections*

We have added a more detailed description of the process for preparing lung models from CT scans.

2. *1.4.1: 100% IPA?*

We have specified that the IPA used in the protocol is ≥99% purity.

3. *1.4.2: mention UV intensity*

We have added the UV oven specifications to the Table of Materials as well as modifying step 1.4.2 below:
Page 5, Line 179: "…cure in UV oven (365 nm light at 5-10 mW/cm^2)…"

***Protocol Highlight:** After you have made all of the recommended changes to your protocol (listed above), please re-evaluate the length of your protocol section. Please highlight ~2.5 pages or less of text (which includes headings and spaces) in yellow, to identify which steps should be visualized to tell the most cohesive story of your protocol steps.*

We have updated the highlighted sections to reflect changes made to the protocol.

***Discussion:** Please ensure that the discussion covers the following in detail and in paragraph form (3-6 paragraphs): 1) modifications and troubleshooting, 2) limitations of the technique, 3) significance with respect to existing methods, 4) future applications and 5) critical steps within the protocol.*

Thank you for this comment. We have revised the discussion section of our manuscript and believe we have addressed all five of these points. Please advise if we have not sufficiently addressed any of these areas.

***Commercial Language:** JoVE is unable to publish manuscripts containing commercial sounding language…Examples of commercial sounding language in your manuscript are Materialise Mimics, Meshmixer, Solidworks, etc.*

Throughout the manuscript, we have replaced all instances of "Materialise Mimics" with "CT scan software," "Meshmixer" with "mesh editing software," and "Solidworks" with "3D modeling software." The Table of Materials has also been updated to reflect these changes.

Reviewer Comments

Reviewer #1:

1) *Authors have followed the work of Sul et al., but at most of the places authors have just cited the paper and not provided necessary information e.g., flow rate, aerosols diameters and other properties (See NOTE given at Line no 226). It would have good to define all the details in the manuscript as well in addition to the citation.*

Thank you for this feedback. The distribution of air flow to each lobe of the lung was calculated by Sul et al. by comparing the volume of each lobe at full inspiration and full expiration as determined by thin-slice computed tomography images of patient lungs. As a result, this method could be extended to specific patients to generate unique flow profiles that, when used in conjunction with a patient-specific lung model, have a greater capacity to predict regional distribution of a therapeutic for the specified patient. The indicated NOTE in the manuscript has been modified to clarify these details:

Page 6, Line 256: "…calculated by Sul et al. using thin-slice computed tomography images of patient lungs at full inspiration and expiration, comparing the relative changes in the volume of each lung lobe. Results are presented for two distinct flow conditions, both at an overall inlet flow rate of 1 L/min. The healthy lung lobe outlet flow profile is distributed to each outlet by the following percentage of the inlet flow: LL-23.7%, LU-23.7%, RL-18.7%, RM-14.0%, RU-20.3%. The COPD lobe outlet flow profile is distributed between each outlet by the following percentage of the inlet flow: LL-10.0%, LU-29.0%, RL-13.0%, RM-5.0%, RU-43.0%."

2) *Figure 3 is provided without mentioning the details of experimental conditions/parameter values.*

Thank you for this comment. The images presented in this figure were collected during an experiment targeting the left lung using 1 micron particles and the endotracheal (ET) tube attachment depicted in Figure 5 at a flow rate of 1 L/min. The Right Upper (RU) Lobe and Left Lower (LL) Lobe filters were used for the low and high deposition examples, respectively. To demonstrate visually a "good" threshold, a range of 43 to 255 was used, producing images identical to those used in our analysis for that experiment. In comparison, the "poor" threshold images were produced using a range of 17 to 255. Reducing the lower limit of the threshold range detects fluorescent signal from the adjacent filter fibers in addition to the particles' signal, leading to an overestimation of particle deposition on the filter. The figure caption was modified to include these details as indicated below:

Page 10, Line 422: "The raw images presented were collected during an experiment to target the left lung using 1 µm fluorescent polystyrene particles at 1 L/min under a healthy breathing profile. The "high" and "low" deposition images depict the LL (23.7% outlet flow) and RU (20.3% outlet flow) Lobe filters, respectively. The "good" threshold, applied with a range of 43 to 255…The "poor" threshold, applied with a range of 17 to 255…"

3) *The results and discussion sections do not provide much information on the flow physics and reasoning for the specific deposition behaviour.*

Thank you for this feedback. We have enhanced our discussion with a number of points raised by both reviewers. Specifically, we have added a discussion paragraph to highlight the importance of geometry and targeting position in the resultant deposition profiles, as shown in the following:

Page 11, Line 461: "As shown in **Figures 4 and 5**, lobe-level deposition can be accurately and rapidly measured for both targeted and non-targeted inhalation aerosols. In the absence of a targeting device, particles in this size range (1-5 µm) and flow conditions (1-10 L/min) follow the fluid stream lines and total airflow profile diverted to each lobe (**Figure 4**). Notably, various inhaler devices and ET tube attachments can be developed to concentrate inhaled medicines to controlled lobe locations. As described in our recent work and those of others, many features of the inhaler device, flow profile, and airway geometry contribute to targeted deposition behavior. In general, efficient regional targeting as demonstrated by our unique *in vitro* models requires a narrow aerosol size distribution and low inhalation flow rates to avoid airway turbulence specifically found within the trachea. Inclusion of the full upper airway within our *in vitro* model allows for accurate recreation these airflow patterns that are known to influence downstream lobe-level distribution. Because of these complex flows, recent work has demonstrated increased targeting from below the glottis. Our results in **Figure 5** specifically highlight the benefit using an ET tube adaptor to regionally target individual lobes from release below the glottis, with efficient lobe-specific targeting shown for lobes of both the right and left lungs at efficiencies ranging between 62-74% of the total dose. This represents an increase over previously experimentally reported mouth-release regional targeting efficiencies and is an important avenue for clinical implementation of this approach. Importantly, the protocol allows for experimental lobe distribution measurements of a complete pharmaceutical dosage from a wide range of potential regional targeting devices beyond those demonstrated here."

4) *No conclusion has been given in the manuscript. Manuscript is written in a very simple way and provides very limited details regarding the experimental outcomes.*

We appreciate this feedback and have tried to enhance our protocol discussion to also reflect the experimental outcomes where appropriate. We have added additional experimental discussion points (see responses to additional reviewer comments) and have augmented the concluding statements to include the following:

Page 13, Line 539: "Our protocol demonstrates the first *in vitro* experimental setup with the ability to quantify lobular pulmonary deposition in a patient-specific lung geometry. Achieving controlled lobe-level distribution is expected to increase therapeutic efficacy of inhalation therapeutics, which will only be achieved through advances in *in vitro* whole-dose measurements. With the growing interest in personalized medicine, this protocol has the potential to spur the development of new targeted lung therapies by allowing for more accurate predictions of potential treatment efficacy."

Reviewer #2:

This work shows a novel methodology based on 3D printing to create patient-specific bronchial tree models to test deposition patterns of pharmaceutical aerosols. The text and figures are illustrative and well structured. Some more details are required, in particular for the 3D printing of the models

and how to perform some quality control over them in terms of accuracy and reproducibility and integrity of the resins used after each experiment.

Further details are required in terms of how the models are 3D printing and testing the integrity of them during the experiments with the aerosols. More details with regard to how to go from CT patient images to the models are needed and also about certain decisions taken for the models such as stopping them at the 2-3 bifurcation instead of going beyond in the bronchial tree.

Thank you for this helpful feedback. We have made multiple additions to the manuscript (detailed below) to touch on these points. Specifically, in our procedure, we have added additional information about the 3D printing method used and the process of preparing models for 3D printing. In our discussion, we have emphasized some additional key limitations of the current lung models used and the current work ongoing in our lab to ameliorate these points, as described in the following.

1) *Page 2, section 1.1.1 and Fig. 1A. Fig 1A is not the CT scan, please modify the title over that particular image, it is a model. Please add to Fig 1 a sagittal slice of the actual thorax scan that was used for that particular model.*

Thank you for this feedback. The suggested change was made to the title in Figure 1A. The particular model used in this study was a generous gift from our collaborator and an in-depth geometrical analysis of this particular model has been previously published, which includes a sagittal slice in addition to other views[1]. Please refer to Figure 8 of the referenced Feng et al. paper, for additional views of the original CT scan and lung model, in addition to a more detailed discussion of geometrical features. We have added the following statement to the manuscript to direct readers to this additional information:

Page 2, Line 86: "NOTE: For a more detailed discussion of the geometrical features of the lung model used in these studies, refer to Feng et al."

2) *Page 3, line 89. Why was the wall extended 2 mm? Is this related to the selected 3D printing technique to guarantee that the printed models will be robust/strong enough or is it linked to the actual wall thickness of the bronchii? Please explain in the text.*

The thickness of the lung model walls was chosen to be 2 mm to adhere to recommended feature sizes for the 3D printer (Carbon M1 Printer) and resin (PR25 resin) used to produce the models. As a result, this thickness could be varied by researchers depending on which instruments and materials are available. Since the protocol uses a rigid model, the wall thickness can be adjusted for the requirements of various 3D printing methods as long as the interior geometry and dimensions of the model are maintained. This does not impact the airspace topography at all. The following statement has been added to the text to clarify this:

Page 3, Line 104: "The thickness of 2 mm was chosen based on the acceptable feature sizes specified by the manufacturer of the 3D printer listed in the Table of Materials. This thickness can be adjusted based on the specifications of the 3D printer available as long as interior geometry of the model is maintained."

3) *Page 3, line 91. In your method, the modelling of the bronchial tree stops at the generations 2 or 3, at the entrance of each of the lobes. Please comment in discussion if this is realistic enough to test the deposition of the pharmaceuticals or if it could be better in the future to generate more vessels in your model to measure more accurately the distribution.*

Thank you for this comment. Our method was developed specifically to address the need for a tool to assess regional deposition at the lobe level. Modeling the bronchial tree up until the lobe entrances allows for the identification of regional differences in delivery while remaining high throughput. Additionally, the clinical data used to validate the flow profiles generated in the model are reported at the lobe level. Since this clinical data was collected *in vivo,* it includes the full lobes and incorporates aspects of the geometry relevant to our analyses. Nevertheless, this is a limitation of our method which warrants further development. There is ongoing work in our research group on developing a method of modeling further generations of the lung without adding a great deal of complexity to the protocol. The following statement has been added to address these points:

Page 12, Line 507: "While these models currently can only replicate patient geometry up to the second or third generation to adequately measure lobe-level distribution, work is ongoing to develop modifications that can incorporate the lower airways for more detailed analysis."

4) *Is there such a big inter patient variation related to sex and race (I can imagine differences due to age, specially for pediatrics), if you only consider bronchial models till the entrance of the lung lobes? Please, give some details in discussion.*

Thank you for this point. Regions of the upper airways including the pharynx, larynx, and trachea can have a significant impact on regional deposition, which varies among subject age, race, and sex. The following addition has been made to the discussion to expand on these points:

Page 12, Line 493: "Differences in lung flow profiles and geometries due to characteristics such as age, race, and sex are well documented in literature[16-18] and can be readily incorporated into our modelling approach. Specifically, geometric variations in the larynx, pharynx, and trachea of lung models can have a significant impact on airflow and subsequent regional deposition patterns[14], which this protocol is well-equipped to detect."

5) *Page 3, section 1.3.1. Please provide more details about the printing materials and the printer used and the printing method (the printer is not mentioned in the Materials table, I believe, just the resins). It is important to mention that the chemical properties of the selected 3D printing materials are relevant, specially in terms of possible interactions with the aerosols or the rinsing liquids used in between experiments.*

Thank you for this feedback. Per JOVE's statement on commercial language, we have kept the protocol to be generalizable to a wide range of 3D printers but have elaborated on your points in the following. The 3D printer and resins used in this protocol are products of Carbon® and use a form of stereolithography (SLA) termed Continuous Liquid Interface Production™ (CLIP). The hard resin used is PR25, a proprietary mixture of photoinitiator and reactive diluents meant for rapid prototyping. It can be exposed to IPA for

up to one hour before impacting the structural integrity of the cured resin. The soft resin used is an elastomeric polyurethane (EPU40), another proprietary composition that allows for the printing of the elastic cap components. Due to this property, EPU40 has a solvent exposure time of only one minute during post processing. However, the parts printed with this resin are not patient-specific and can be easily replaced in the event of wear-and-tear due to stretching or solvent exposure. This protocol follows all manufacturer instructions with respect to these resins and can be easily adapted for compatibility with other brands or classes of materials. Links to manufacturer information on both of these resins was added to the Table of Materials. In addition to the printer and resins, other post-processing tools, including the convection and UV ovens used, were added to the Table of Materials. In the text, we have included additional references to the Table of Materials and added the following note:

Page 4, Line 166: "NOTE: All post-processing steps described below are specific to the 3D printer listed in the Table of Materials. When utilizing alternate printers or materials, adjust these steps to reflect manufacturer instructions."

6) *Did you test the accuracy and/or reproducibility of the 3D printing process and your models? It would be interesting to scan the model with a protocol similar to the one used for the patient and compare the images. Even though the attenuation properties of the resin will be different, this experiment can give insight about how similar is your final product to the actual patient.*

Thank you for this comment, the suggestion of imaging the model to quantify the accuracy of the printing process will be incorporated into this paper and future projects. The process of using CT scans to generate a 3D rendering to be printed using the Carbon M series printers has been FDA approved[6] for medical use and, thus, we did not previously investigate the accuracy of the print due to the proven accuracy in these specific prints. However, we recognize the benefit of confirming that this process is as accurate as we assumed it to be, and would recommend the use of a µCT (Micro-Computed Tomographic scan) to perform this characterization due to the small size of the replica. This has been included in the following statement:

Page 5, Line 182: "Note: To evaluate the accuracy of the 3D printed replica, we recommend the use of µCT scanning the printed part and using CT scan software to compare, quantitatively, variations between the original 3D rendering and the 3D printed replica."

7) *Page 7, line 280 (Note): In between experiments, it is stated that the 3D printed tree is rinsed with isopropyl alcohol. Plastics tend to be quite sensitive to light exposure and subject to chemical interactions. Have you tested the durability of your models and their integrity after several experiments? Have you considered designing a sort of quality control procedure to check one model cannot be used anymore?*

Thank you for this value comment. We agree with the potential sensitivity to plastic parts to various solvents, including IPA. Per the manufacturer, the Carbon resin used for the airway replicas is PR25 which has a maximum IPA exposure time of one hour per manufacturer instructions. However, only a few minutes of exposure is required to complete the initial post-processing cleaning, and the exposure time during experiments referenced in the note on Page 7 Line 280 is 10-15 seconds. Additionally, more than

one replica was created for this work. Therefore, we estimate that the total exposure time of any one replica is less than 10 minutes, which does not approach the IPA limit. We recommend use of an exposure log to track the use of a model and ensure the exposure limit is not approached. This information has been included in the below statement:

Page 8, Line 318: Note: "...Additionally, a log is kept to ensure all replicas used have been minimally exposed to IPA to maintain part integrity and visual part inspection is recommended prior to use."

8) *Page 8, line 325. Please add the size range here.*

We have added the size range (1-5 µm) on page 8.

9) *Page 8, line 336. Your method reproduces the distribution of the air flow till the entrance of the lung lobes, not on all the lungs. Please modify the statement.*

We have altered the specified statement as shown below:

Page 9, Line 383: "…distribution of air flow to each of the lung lobes."

10) *Figure 3. Please give some details about what is a "good" threshold and a "bad" threshold, even for the particular case you show. If someone tries to reproduce your experiment they would need this information.*

Thank you for this feedback. The critical difference between a "good" threshold and a "poor" threshold is the amount of signal detected from the filter paper fibers rather than the particles themselves. Although the filter paper does not have any inherent fluorescence, the fibers can diffract light, obscuring the borders of large deposits of fluorescent particles. To clarify this distinction and aid in identifying a proper threshold range, we have added more detail to the figure caption and added an additional note as shown below:

Page 10, Line 426: "The 'good' threshold, applied with a range of 43 to 255, maintains defined edges between individual particles and avoids detection of filter paper fibers. The 'poor' threshold, applied with a range of 17 to 255, obscures individual particle borders and overestimates the fluorescent area of the filter."

Page 9, Line 352: "NOTE: For filters with high levels of deposition, a 'corona' of fluorescence, caused by the diffraction of light by the filter paper fibers, may be observed around large groupings of particles. When thresholding these images, a range that is too large displays small dots or 'feather-like' shapes around these groupings, as observed in the 'poor' threshold images in Figure 3. This can be improved by gradually increasing the lower limit of the threshold until the signal from the filter paper fibers is minimized without obscuring the signal from the particles themselves."

11) *Page 10, line 404. It is stated that the proposed protocol can be used to create patient-specific models and thus test the influence of anatomical differences in age, race, sex in the deposition of the aerosols. Nonetheless, the proposed models only expand for a few bifurcations in the bronchial tree. Please explain the validity/limitations of your approach and also if in some studies it would be better to have a larger range of bronchii to simulate a more realistic air flow and aerosol deposition.*

Thank you for this comment. Please see our responses to comments 3 and 4 above.

12) *Page 10, line 410. Please, comment on discussion about the costs of the 3D printed models that are used in your work and how feasible would it be to do it routinely for clinical trials.*

Each lung model requires about 130 mL of PR25 resin to produce. At $0.12/mL of PR25 resin, a lung model can be produced for only $15. The most significant cost associated with the production of these lung models is the 3D printer itself and its associated software; however, 3D printers are becoming increasingly prevalent in hospitals worldwide for diagnostic and surgical planning purposes[7]. In the United States and Canada alone, over 113 hospitals have 3D printers on-site. For hospitals with an existing 3D printing infrastructure, producing a large number of lung models for a clinical trial would be relatively low cost. We have added the following statement to touch on this topic:

Page 12, Line 485: "This protocol will not only provide an experimental lab-scale approach to support design of new inhaler devices, but also create opportunity for on-demand personalized inhalation devices in clinical practice. The hard resin used in this protocol costs ~$0.12/mL; therefore, hospitals with existing 3D printing infrastructure could print a lung model for as little as $16 in materials[15] and assemble a personalized airway in under a day. Notably, printing times and material costs in additive manufacturing continue to decrease rapidly, increasing the overall feasibility of this approach."

13) *Page 10, line 426. The authors explained nicely the possible differences in the behavior of the selected resin and the actual tissues in patients. Please add a sentence of the potential possibility in the future to use 3D printed materials that actually mimic patient tissue, such as has been already done with skin. 3D printing is a fast moving field and new materials are continuously released. Please add some sentences about the properties (chemical, mechanical...) that a material would require ideally to create the best possible phantom for your application.*

Thank you for this comment. Bioprinting has great potential to incorporate further patient-specificity into the lung models; however, the lung epithelium is highly complex, with great diversity in cell types, making it very difficult to develop an accurate bioprinted mimic. Most pulmonary bioprinting work, thus far, has been focused on small structures such as organoids or grafts[8]. Nevertheless, we are investigating other methods of incorporating a cellular response into our analysis such as culturing cells on 3D printed materials. The following statement has been added to the discussion:

Page 12, Line 523: "Other techniques such as bioprinting and culturing cells on 3D printed models are being investigated for their ability to incorporate a cellular response into the protocol"

14) Page 1, line 32. Typo: "This protocol has the potential promote..." Please add "to" in front of promote

We have made this change on page 1.

References in this Response Document

1. Feng, Y., Zhao, J., Chen, X. & Lin, J. An In Silico Subject-Variability Study of Upper Airway Morphological Influence on the Airflow Regime in a Tracheobronchial Tree. *Bioengineering*. **4** (4), 90, (2017).

2. Feng, Y. *et al.* An in silico inter-subject variability study of extra-thoracic morphology effects on inhaled particle transport and deposition. *Journal of Aerosol Science.* **123** 185-207, (2018).

3. Martin, S. E., Mathur, R., Marshall, I. & Douglas, N. J. The effect of age, sex, obesity and posture on upper airway size. *European Respiratory Journal.* **10** (9), 2087, (1997).

4. Jiang, Y.-Y., Xu, X., Su, H.-L. & Liu, D.-X. Gender-related difference in the upper airway dimensions and hyoid bone position in Chinese Han children and adolescents aged 6–18 years using cone beam computed tomography. *Acta Odontologica Scandinavica.* **73** (5), 391-400, (2015).

5. Weber, P. W., Price, O. T. & McClellan, G. E. Demographic Variability of Inhalation Mechanics: A Review. (Defense Threat Reduction Agency 2016).

6. "KeySplint Soft™ Clear by Keystone Industries®, a Unique 3D Printing Resin for Night Guards and Splints Available Exclusively on the Carbon® Digital Manufacturing Platform, Cleared for Sale by U.S. FDA." Carbon, 18 November 2019. Press Release.

7. Pietila, T. *How Medical 3D Printing is Gaining Ground in Top Hospitals*, <https://www.materialise.com/en/blog/3D-printing-hospitals> (2019).

8. Galliger, Z., Vogt, C. D. & Panoskaltsis-Mortari, A. 3D bioprinting for lungs and hollow organs. *Translational Research.* **211** 19-34, (2019).